Determination and Analysis of Working Diameters and Working Angle of the Torus Cutter Blade in Multi-axis Machining in the Aspect of Tool Wear

Michał Gdula

Department of Manufacturing Techniques and Automation, Faculty of Mechanical Engineering and Aeronautics, Rzeszow University of Technology, 35-959 Rzeszow, al. Powstańców Warszawy 12, Poland
Email: gdulam@prz.edu.pl

***Abstract*—The aim of this study is to provide a theoretical and experimental analysis of the multi-axis milling process by the torus milling cutter of nickel-based superalloy parts in terms of surface quality and tool wear. In the analytical part, using, among other things, matrix calculus and trigonometric relationships, mathematical models were developed to describe the relationships between the tool axis orientation and the geometric parameters of the cutting layer at the contact point. On this basis, mathematical relationships for contact diameter and effective diameter were derived. The basis for these considerations is the very rarely considered working angle of the cutter blade. In part of the experimental study, machining tests were carried out for selected kinematic variants of multi-axis cutting. Based on the results obtained, it was found that as the tool axis inclination angle increases, the contact diameter increases. The effective diameter at the upper characteristic point of the cutting layer increases up to a certain angle of inclination, after which it begins to decrease. The rotational angle of the tool axis does not affect any of the diameters, but it does affect the displacement of the contact point, the values of the working angle of the tool blade and the feed-related component decrease. The result of this displacement is a change from climb milling to conventional milling, which has significantly degraded surface quality and tool life. The best results of the machining test were obtained when only the angle of inclination of the tool axis was used. It was concluded that the parameter tool blade working angle can be a control variable in a multi-axis milling process and has a major impact on the physical aspects of the cutting process.**

***Keywords*—torus milling cutter, effective diameter, contact diameter, multi-axis machining, cutter blade working angle, tool wear, surface roughness**

I. Introduction

Multi-axis torus milling cutter machining of sculptured surfaces parts made of Ni-based superalloy is one of the increasingly used technologies for precision finishing. This is primarily due to the advantages that the torus geometry has. It enables the milling width to be significantly increased, making the machining process more efficient while maintaining the required quality indicators of the machined surface. In addition, zero-speed cutting does not occur with a torus milling cutter geometry, which is the case with a ball-end milling cutter geometry [1–6]. Essentially, the cutter rotates around its axis and moves to shape the surface by following a movement trajectory programmed in the Computer-Aided Design/Computer-Aided Manufacturing (CAD/CAM) system at a specific speed (feed rate, v_f) and finally moves away and u-turns or departs.

In the case of multi-axis milling of sculptured surfaces using a torus milling cutter (as well as using a ball-end milling cutter, which is the subject of the vast majority of the research work in the theme of this paper), the surface quality indicators depend on several factors and parameters, such as: essential diameter, effective diameter, contact diameter, cutting parameters, cutting blade and workpiece materials, machined surface geometry, toolpath, kinematic variant of multi-axis cutting process, etc. The parameter that links all of the above with surface quality indicators is tool wear.

Regarding the essential diameter and effective diameter of the tool, Fan [7] conducted a study on the effect of variations in cutting speed on the quality of the machined surface. He also noted that cutting speed is a significant factor in tool wear. On the other hand, de Souza *et al.* [8] carried out a study of the influence of effective diameter on surface roughness and selected mechanics of the cutting process, i.e., chip formation, curl and breakage, and cutting forces. He indicated that an increase in the cutting speed results in a decrease in the value of the surface roughness parameters. Wojciechowski *et al.* [9] analysed the milling process using the ball-end mill cutter of planar surfaces inclined at different angles, resulting in different effective diameters. They indicated that the larger the effective diameter, the lower the surface roughness, while an increase in the cutting speed results in a decrease in the value of the surface roughness parameters. In addition,

Manuscript received February 26, 2024; revised April 6, 2024; accepted May 28, 2024; published October 17, 2024.

Wojciechowski *et al.* in their work [10, 11] extended the scope of the study to include the determination of geometrical parameters of the machined layer in different phases of blade operation, indicating their influence on the components of the cutting force taking into account tool wear. In turn Mikó *et al.* [12] and Mgherony *et al.* [13], they presented the geometrical basis of the 3-axis milling process with a spherical milling cutter for free-form surfaces. Based on the results of research, they formulated assumptions for a ball-end milling strategy that minimises changes in instantaneous effective diameter values.

Regarding tool material, workpiece, and cutting kinematics, Vopát *et al.* [14] conducted a study of the influence of tool material and milling direction on quality indicators of machined surface and tool wear. They indicated that the solid carbide cutter provides better surface roughness and blade life than the HSS mill. Furthermore, for both tool materials, milling in the kinematic variant push the tool provides better surface roughness. In the works of Wojciechowski *et al.* [9–11], a similar kinematic range of milling was performed and the workpiece material was hardened steel. The kinematics of multi-axis cutting is closely related to the inclination parameter of the tool axis or machined surface, so Vyboishchik [15] described a geometric model of the topology of a flat surface and a convex and concave curvilinear surface. On this basis, he assessed that the angle of inclination of the surface at the local contact point plays an important role in the milling process of free-form surfaces.

Regarding milling strategies and parameters, Beno *et al.* [16] conducted a study of milling strategy selection based on the analysis of complex surface features. He noted that cutting speed has a major impact on the quality indicators of the machined surface. Pena e*t al.* [17] conducted a study of different milling strategies in terms of the surface roughness achieved. Due to the different roughness values obtained, they introduced a correction factor that modifies the feed rate to ensure better surface quality indicators. On the other hand, Pena [18] also analysed different milling strategies, found that the calculated roughness height was smaller than its actual value, and proposed a correction factor to modify the cutting width. Redonnet *et al.* [19] carried out an optimisation of a milling strategy for free-form surfaces using a torus cutter, minimising machining time using a kinematic roughness height criterion. Zhang *et al.* [20] developed a geometric model of the topography of a surface machined using a ball-end mill. They performed the optimisation by taking into account the effect of the feed rate on the tooth and the cutting width.

The process of simultaneous multi-axis milling can solve an existing problem in optimising tool life extension, resulting, among other things, from the occurrence of variable effective diameters and therefore cutting speeds during machining. As pointed out by Zhang *et al.* [1], cutting speed has a major impact on tool wear. By combining the simultaneous multi-axis milling technique with the 3+2 milling technique while introducing the technique of segmenting the machined surface and/or cutting edge by varying the inclination of the tool axis, this problem can be largely overcome. Liu *et al.* [21] developed a workpiece surface segmentation method to identify regions for a 3+2-axis milling strategy. They pointed out that this technique, due to the static axis of the tool in three-dimensional space, allows for increased feed rates. On the other hand, Gdula *et al.* [22] determined the basic kinematics variants of multi-axis cutting in terms of segmentation of the cutting edge of a torus cutter. They conducted a series of milling tests for different tool axis inclinations, determining their effect on tool wear and the morphology of the chip and machined surface. This work provides a starting point for the research within this thesis.

In summary, the surface quality according to the geometric model depends on the diameter of the tool, the cutting width, and the tool axis inclination of the tool axis, as well as on the cutting parameters such as feed and cutting speed. When sculptured surfaces, the effective diameter of the cutting tool changes, and thus the cutting speed also changes. In turn, the cutting speed determines the minimum value of the chip thickness.

This paper emphasises engineering aspects in the context of CAD/CAM programming support, taking into account the tool wear parameter. As can be seen from the analysis of the literature, the cutting speed has a significant effect on the wear of the tool and thus on surface roughness. In the case of multi-axis torus milling cutter machining, the effective diameter is a key research parameter. In addition, the novelty of this work is the inclusion of the diameter at the point of contact (contact diameter), as that which shapes the machined surface through the direct cutting edge-machined surface contact. Furthermore, this work is distinguished by its geometric-kinematic approach to the description of the aforementioned diameters and other related parameters. The mathematical model developed describes the multi-axis milling of a surface using the torus milling cutter with a variable inclination of its axis, where the tool paths are parallel to each other. The machined surface is a tangent plane, which is a simplified model of a sculptured surface at the contact point between the torus and the machined surface, as shown in Fig. 1. The necessary simulations were performed on the developed model relationships and the discrete direct CAD method in the CAD/CAM environment.

This study is an extension of the geometrical approach used for 3-axis ball-end milling process [12, 13, 23–26]. Among other things, the novelty of this work is the consideration of the kinematics of the 5-axis milling process at the contact point between the tool and the machined surface, by introducing a working angle of the blade parameter. This parameter was used to determine the effective and contact diameters, which, according to the literature analysis, is the first of its kind given the modelling of the multi-axis milling process. In addition, the milling cutter working angle blade parameter was used as a control variable when programming the milling

cutter axis inclination angle as well as during the implementation of the experimental tests. All tests and analyses were carried out for the torus milling cutter, for which there are no studies in the above area.

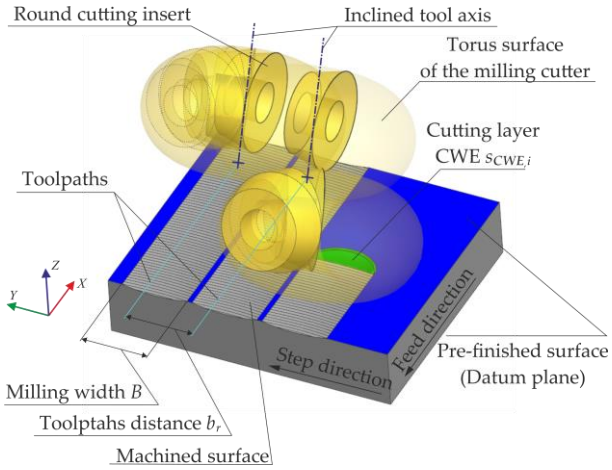

Fig. 1. Milling of the plane surface with inclined torus milling cutter axis.

II. Contact and Effective Diameters

Let the reference coordinate system (X_{ci}, Y_{ci}, Z_{ci}) be located at point O_{ci} of the circular outline centre of the cutting edge of the cutting insert and the coordinate system (X_{CPi}, Y_{CPi}, Z_{CPi}) at the contact point CP_i. The Z_{ci} axis is constant in terms of direction and the turn of the axis, and is parallel to the normal vector N of the machined surface. The parameter D_{PRIN} indicates the tool's principal diameter. Furthermore, let the angle δ be the angle of inclination of the tool axis and let the angle θ be the angle of rotational of the tool axis, relative to the normal vector N at the CP_i contact point. The parameters δ and θ are the spherical coordinates of the tool axis, as shown in Fig. 2.

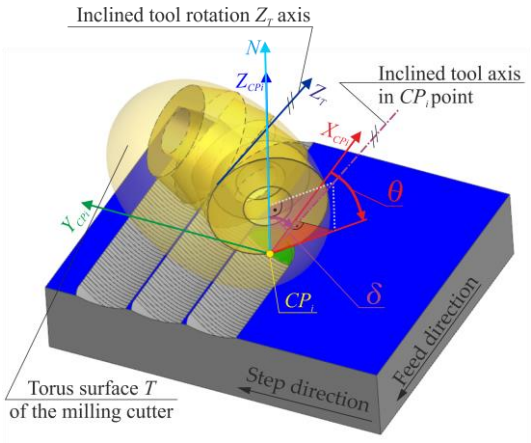

Fig. 2. Directional versor k of the torus milling cutter axis and its spherical coordinates: inclination angle δ and rotational angle θ at the CP_i contact point.

A. Contact Diameter

1) Case I: $\delta=0°$ and $\theta=0°$

If R_T is the radius of the torus milling cutter (the Z_T rotation axis of distance of the torus from the centre of the circle defining it), the contact diameter at the contact point CP_i is described by Eq. (1) (see Fig. 3(a)):

$$D_{CON\,I} = 2R_T \tag{1}$$

2) Case II: $\delta>0°$ and $\theta=0°$ or $-90°<\theta<90°$

However, in addition, if r_p is the radius of the circular cutting insert (the circle defining the torus) and R_T, δ and θ as described above, the contact diameter at the CP_i contact point is described by Eq. (2) (see Fig. 3(b)):

$$D_{CON_{II}} = 2\left(R_T + r_p \sin(\delta)\right) \tag{2}$$

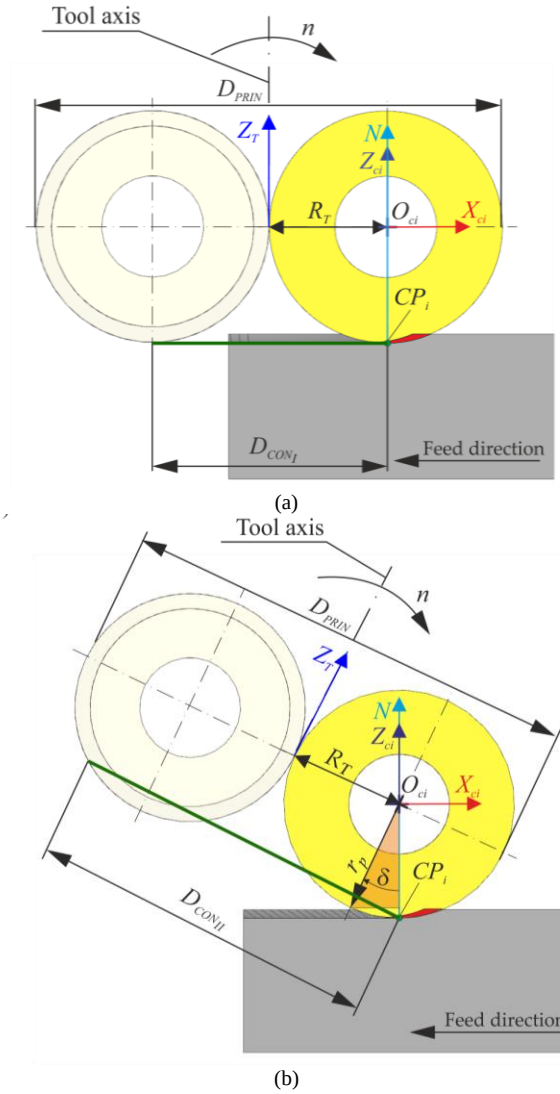

Fig. 3. Definition of the contact diameter in the $X_{ci}Z_{ci}$ plane: (a) case I: $\delta=0°$ and $\theta=0°$, (b) case II: $\delta\neq0°$ and $\theta=0°$ or $\theta\neq0°$.

B. Effective Diameter

1) Specific case: The cutting edge tangential to the machined surface at the contact point CP_i

In the multi-axis cutting process with the torus milling cutter used, the cutting speed v_c depends not only on the spindle rotation speed n and the principal diameter D_{PRIN}, but also on the axial depth of cut a_p, the inclination angle

δ and the rotational angle θ of the tool axis. The cutting speed will reach its maximum value when, in a given kinematic variant of multi-axis cutting, the active cutting edge is tangential to the contour of the machined surface (generalising: machined plane) at the contact point CP_i. In this particular position of the geometrical-kinematic tool-workpiece relationship (CWE), due to the maximum value of the axial depth of cut a_{p_max}, the effective diameter also has a maximum value.

To calculate the maximum value of the cutting speed, Eq. (3) applies:

$$v_{c\_max} = \frac{\pi \cdot D_{eff\_max} \cdot n}{1000} \tag{3}$$

In Eq. (3), D_{eff_max} denotes the maximum effective diameter of the tool (considered in the base plane P_r in the tool layout), as shown in Fig. 4.

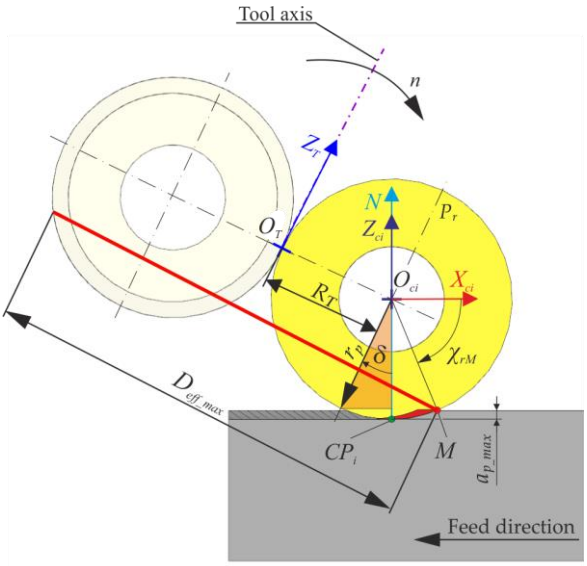

Fig. 4. Definition of the maximal effective diameter in the multi-axis milling process using the torus milling cutter.

In order to determine the equation of the maximum effective diameter D_{eff_max}, assumptions were made as described above. The components in the direction of the X_{ci} and Z_{ci} axes of the adopted reference coordinate system (O_{ci}, X_{ci}, Y_{ci}, Z_{ci}), i.e. the cutting blade system, were then determined, as shown in Fig. 5. The x and y components are described by the system of Eq. (4):

$$\begin{cases} x = r_p \cos(\chi_{rM}) \\ y = r_p \sin(\chi_{rM}) \end{cases} \tag{4}$$

Due to the inclination of the torus cutter axis by an angle δ, the components of the system of Eq. (4) were transformed, that is, rotation by an angle δ. Therefore, in the next step of the calculation another counterclockwise rotation of these components by angle δ was performed. This is to bring the components from the cutting tool system to the cutting blade system.

Therefore, the rotation matrix takes the form in Eq. (5):

$$R(-\delta) = \begin{bmatrix} \cos(-\delta) & -\sin(-\delta) \\ \sin(-\delta) & \cos(-\delta) \end{bmatrix} \tag{5}$$

This matrix rotates the column vectors according to Eq. (6):

$$\begin{bmatrix} x' \\ y' \end{bmatrix} = \begin{bmatrix} \cos(-\delta) & -\sin(-\delta) \\ \sin(-\delta) & \cos(-\delta) \end{bmatrix} \cdot \begin{bmatrix} x \\ y \end{bmatrix} \tag{6}$$

Hence, the x' and y' components, when transformed, take the form of a system of Eq. (7):

$$\begin{cases} x' = r_p \cos(\chi_{rM}) \cos(-\delta) - r_p \sin(\chi_{rM}) \sin(-\delta) \\ y' = r_p \cos(\chi_{rM}) \sin(-\delta) - r_p \sin(\chi_{rM}) \cos(-\delta) \end{cases} \tag{7}$$

The component in the direction of the X_{ci}, axis is important in this case, so ultimately the formula for the maximum effective diameter, taking into account the axis inclination of the torus milling cutter and the axial depth of cut, takes the form in Eq. (8):

$$D_{eff\_max} = 2\left[R_T + \begin{pmatrix} r_p \cos(\chi_{rM}) \cos(-\delta) - \\ - r_p \sin(\chi_{rM}) \sin(-\delta) \end{pmatrix} \right] \tag{8}$$

In Eqs. (4), (7) and (8), the symbol χ_{rM} denotes the final position angle of the boundary point M of the cutting layer cross-section at the cutting edge relative to the X_{ci} axis in the cutting blade coordinate system.

2) Cutting blade work angle

Due to the shape of the cutting edge of the torus milling cutter, the value of the cutting speed varies along the length of its active segment of the cutting edge. During multi-axis milling (all kinematic cases for combinations when $\delta>0°$ and $\theta=0°$ or $\theta\neq0°$), the cutting speed varies from a certain minimum value at point E to a certain maximum value at point M. As can be seen from the kinematics of the multi-axis milling of the torus milling cutter, in the range of the cutting blade work angle $\psi_r(\Omega)$, point M moves along the active segment of the cutting edge, moving away from or closer to the point E (see Fig. 5).

Points E and M are the boundary points of the cross-section of the CWE $s_{cwe,i}$ cut layer. In addition, these points, together with the O_{ci} point of the adopted reference coordinate system, form the outline of the circle cutout $O_{ci}EM$ in the base plane P_r of the round cutting insert of torus T. The circle cutout angle $O_{ci}EM$ is the cutting blade work angle in the base plane P_r, which depends on the tool rotation angle Ω, which is denoted by $\psi_r(\Omega)$. In order to determine the cutting blade work angle, the angles describing the position of the boundary points of the cross-section of the cut layer relative to the X_{ci} axis of the adopted reference coordinate system were determined.

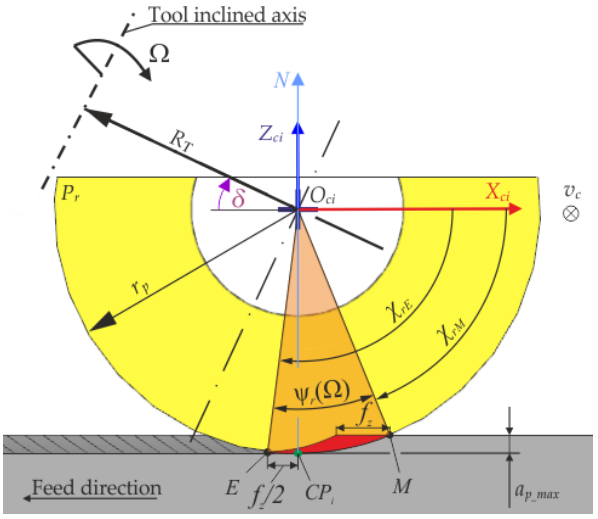

Fig. 5. Geometry of the cutting layer CWE $s_{cwe,i}$ along the cutting edge.

Based on the trigonometric relationships shown in Fig. 5, the value of the angle χ_{rM} of the position of the boundary point *M* is described by Eq. (9):

$$\chi_{rM} = \arcsin\left(1 - \frac{a_{p\_max}}{r_p}\right) \tag{9}$$

In turn, the value of the angle χ_{rE} of the position of the boundary point *E* is described by Eq. (10):

$$\chi_{rE} = \frac{\pi}{2} + \arcsin\left(\frac{f_z \sin\theta}{2r_p}\right) \tag{10}$$

Hence, the value of the cutting blade working angle $\psi_r(\Omega)$ in the base plane P_r, which depends on the tool rotation angle Ω, is expressed by Eq. (11):

$$\psi_r(\Omega) = \left(\frac{\pi}{2} + \arcsin\left(\frac{f_z \sin\theta}{2r_p}\right) - \arcsin\left(1 - \frac{a_{p\_max}}{r_p}\right)\right) \tag{11}$$

For further considerations, the assumption is made that the angle Ω of tool rotation assumes the value $\Omega=0°$, i.e., the outline of the cutting edge is tangent to the outline of the machined surface at the contact point CP_i. Hence, due to the parameter a_{p_max}, the value of the cutting blade work angle $\psi_r(\Omega)$ is the maximum value in this particular case under consideration, and will be denoted as ψ_{r_max} for further consideration.

In conclusion of this section, it should be mentioned that the spherical coordinate in the form of the angle of rotation θ does not affect the value of the contact diameter and the effective diameter, but rather its position in Euclidean space, where the common point of each position of these diameters is the contact point CP_i and the boundary point *M*, respectively. Hence, on the basis of this kinematic property, the distance between the extreme points of the contact curve was determined in the next step.

In Fig. 6, a general example of the considerations to date is shown. The actual effective diameter is the distance between the centre of the torus and the circle of contact. This distance depends on the kinematic variant of multi-axis cutting and the direction of milling.

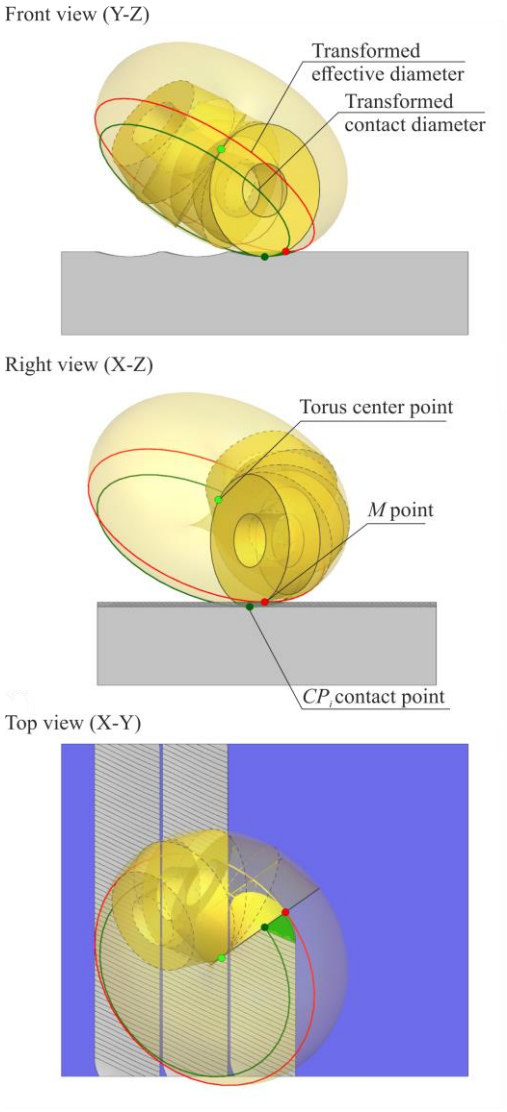

Fig. 6. An example: 3 projected views of the torus milling cutter and the transformed diameters.

III. Determining Distance between the Intersection Points of Contact Curve and Pre-finished Surface

In the transformed contact circle (contact diameter), using analytical geometry and trigonometric relationships, in the *Y-Z* plane, the length of the chord defined by the points t_1 and t_2 can be calculated, as shown in Fig. 7. These are the points of intersection of the contact circle with the machined surface (assumed plane). In the geometrical-kinematic system adopted, there are only two such points. Given the parameters δ and θ, three cases should be considered.

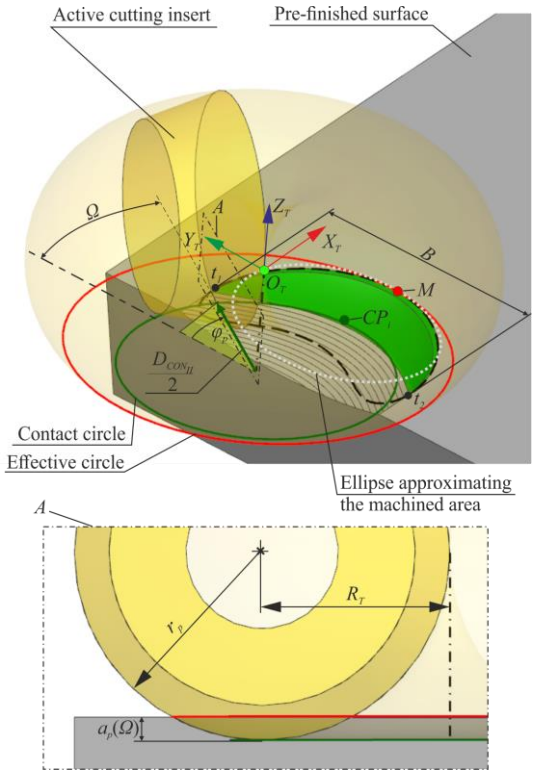

Fig. 7. Determination of milling width *B*.

A. Case I: $\delta=0°$ and $\theta=0°$

If $D_{CON_{II}}/2$ is the radius of the contact circle, $a_{p\_max}=a_p(\Omega)$ is the maximum axial depth of cut, the R_T is the radius of the torus milling cutter, and if r_p is the radius of the circular cutting insert (the circle defining the torus), the milling width *B* is described by Eq. (12):

$$B = 2\left(R_T + \sqrt{2r_p a_{p\_max} - (a_{p\_max})^2} \right) \tag{12}$$

In this case, the contact point CP_i moves in the direction of a rectilinear toolpath perpendicular to the segment defined by the points t_1t_2, thus obtaining the greatest milling width used the torus milling cutter.

B. Case II: $0°<\delta<\left[90-\left(\frac{90-\chi_{rM}}{2}\right)\right]°$ and $\theta\neq0°$

If $D_{CON_{II}}/2$ is the radius of the contact circle, $a_p(\Omega)$ is the the axial instantaneous depth of cut dependent on the angle of rotation of the tool, r_p is the radius of the circular cutting insert (the circle defining the torus), and the φ_p is the cut initial working angle of the torus milling cutter, the milling width *B* is described by Eq. (13):

$$B = 2\left[\frac{D_{CON_{II}}}{2} \cdot \cos(\varphi_p) + \left(\sqrt{2r_p a_p(\Omega) - a_p(\Omega)^2} \right) \cos(\varphi_p) \right] \tag{13}$$

The values of the parameters $a_p(\Omega)$ and φ_p, for a given angle δ of the cutter axis within the given range, are determined using the discrete direct CAD method.

In the third case, i.e. when also $\theta>0°$ (*DP TPL-diagonally positive tool pull*) or $\theta<0°$ (*DN TPL-diagonally negative tool pull*), the determination of the milling width *B* is carried out in a similar way as above, with the additional reliance on an ellipse approximating the machined area.

IV. Research Conditions

Based on the developed geometrical-kinematic model, this section presents adopted conditions of simulation studies and experimental investigations for three kinematic variants of multi-axis cutting: Tool Pulling (TPL), Diagonal Positive Tool Pulling (DP-TPL) and Diagonal Negative Tool Pulling (DN-TPL). Simulation studies were carried out in a CAD/CAM environment using the discrete direct method.

A. Changing Contact Diameter, Effective Diameter and Cutting Speed

Tests in stage one shows the change of values in contact diameter, effective diameter, and cutting speed. In the case shown, the tool's principal diameter D_{PRIN} is 16 mm, the radius of the round cutting insert is 4 mm, and the depth of cut is 0.5 mm. The spindle speed *n* was 1989.43678 1/min, making the cutting speed at the periphery of the principal diameter v_{c_PRIN} equal 100 m/min. In order to avoid the influence of the toolpath distance b_r on the character of the time courses of the tested output quantities, the values of the milling width *B* were smaller than b_r (see Fig. 1). The variable parameters were the inclination angle δ and the rotational angle θ of the tool axis. A detailed summary of the quantities studied in this phase of the research is shown in Tables I and II.

TABLE I. Machining Simulation Parameters, Case $\delta\geq0°$ and $\theta=0°$

Inclination angle δ [°]	Rotational angle θ [°]	Cutting speed v_{c_PRIN} [m/min]	Feed per tooth f_z [mm/z]	Depth of cut a_{p_max} [mm]
$\Delta = 0$ as long as $\delta <$ 90 perform $\delta = \delta+$	0	100	0.25	0.5

TABLE II. Machining Simulation Parameters, Case $\delta=10°$ and $-90°\leq\theta\leq90°$

Inclination angle δ [°]	Rotational mangle θ [°]	Cutting speed v_{c_PRIN} [m/min]	Feed per tooth f_z [mm/z]	Depth of cut a_{p_max} [mm]
10	$\Theta = -90$ as long as $\theta < 90$ perform $\theta = \theta+5$	100	0.25	0.5

B. Changing the Working Angle of the Tool Blade

On the next hand, in the second stage, the study shows, in the first case, the variation of the tool blade working angle ψ_r as a function of the depth of cut and feed per

blade for the kinematic variant of *TPL*-type multi-axis cutting, and as a function of the rotational angle θ of the tool axis for the kinematic variants of *DP-TPL* and *DN-TPL* multi-axis cutting in the second case. To carry out this simulation study, analogous assumptions and values of the variables under study were used as in stage one. A detailed summary of the quantities studied in this phase of the research is shown in Tables III and IV.

TABLE III. MACHINING SIMULATION PARAMETERS, FIRST CASE

Inclination angle δ [°]	Rotational angle θ [°]	Cutting speed v_{c_PRIN} [m/min]	Feed per tooth f_z [mm/z]	Depth of cut a_{p_max} [mm]
10	0	100	0.25	0.3 0.4 0.5
10	0	100	0.15 0.20 0.25	0.5

TABLE IV. MACHINING SIMULATION PARAMETERS, SECOND CASE

Inclination angle δ [°]	Rotational mangle θ [°]	Cutting speed v_{c_PRIN} [m/min]	Feed per tooth f_z [mm/z]	Depth of cut a_{p_max} [mm]
10	θ=15 as long as θ<165 perform θ=θ+5	100	0.25	0.5

C. Experimental Investigation of the Multi-axis Milling Process Using the Torus Milling Cutter

The experimental set-up is shown in Fig. 8. A vertical 5-axis CNC machining centre (DMU 100 MonoBLOCK) is used to conduct the multi-axis milling tests. Test material is Ni-based superalloy Inconel 718.

The multi-axis milling process was conducted by applying steel torus milling cutter body R300-016A20L-08L for indexable round cutting inserts R300-0828E-PL. The body of the torus milling cutter has a neutral geometry. Round cutting inserts are made of S30T cemented carbide grade. Grade S30T has fine-grain cemented carbide and a TiAlN Physical Vapor Deposition (PVD) coating. The round cutting inserts used in the tests have the following parameters: the rake angle is 20°, the relief angle (or else clearance) is 15° and the insert radius is 4 mm.

Furthermore, the cutting insert does not have a typical roundness radius r_ε of the cutting edge, but an asymmetrical chamfer with the following dimensions: length 0.1 mm measured along the line of intersection of the reference plane and orthogonal plane, and an angle of 15° measured in the orthogonal plane between the edge of the chamfer and the line of intersection of the reference plane and orthogonal plane in the Orthogonal Rake System (ORS) of the tool geometry. These 8 mm diameter round cutting inserts was attached in to a 16 mm diameter tool body at an overhang measuring 65 mm.

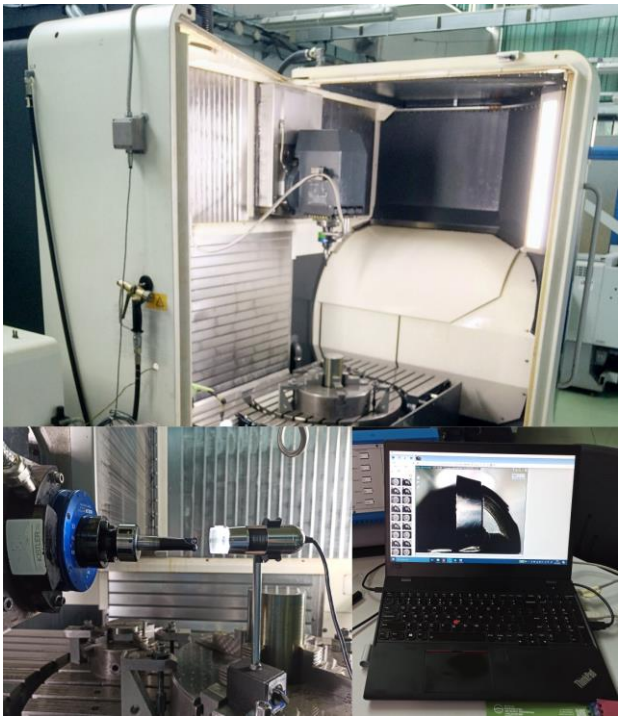

Fig. 8. Experimental test bench.

Multi-axis milling parameters are presented in Table V. In this parameters consist of: the cutting parameters and the tool axis orientation parameters. The cutting parameters were assumed to be constant and invariant for each experiment. Their values were chosen based on recommendations from the tool manufacturer and the aerospace industry. Hence, it was decided to keep the cutting speed values within the speed range for High Speed Machining (HSM) cutting with regard to Ni-based superalloys. The input variables were the tool axis orientation parameters, i.e., inclination angle δ and rotational angle θ. Flood cooling was used in each experiment, and starting each new experiment, the round cutting inserts were replaced with a new set. The tool life was determined on the basis of the localized flank wear (VB_{max}), until it reached 0.3 mm. This was to avoid the effect of excessive tool wear on the workpiece surface due to the higher temperature. The multi-axis milling process was interrupted at specific intervals to identify the wear patterns and measure the wear rate by using a Dino-Lite 7000 CE series digital workshop microscope. Selected 2D and 3D roughness paramaters of the shaped surfaces at the CP_i contact points were measured non-contact using Alicon's InfiniteFocus optical microscope.

TABLE V. MULTI-AXIS MILLING PARAMETERS

Experiment No.	Inclination angle δ [°]	Rotational angle θ [°]	Cutting speed v_{c_PRIN} [m/min]	Feed per tooth f_z [mm/z]	Depth of cut a_{p_max} [mm]	Milling width B [mm]	Toolpaths distance b_r [mm]
1	21.26157	−63.05383				5.3587	5.8
2	21.26157	63.05383	100	0.25	0.5	5.3587	5.8
3	10.00000	0.00000				9.1191	9.3

V. Result and Discussion

A. Changing Contact Diameter, Effective Diameter and Cutting Speed

1) Case, $\delta \geq 0°$ and $\theta = 0°$

A study was first carried out for the case in which the machining parameters, i.e. rotation speed and cutting speed, were set relative to the principal diameter D_{PRIN}. Fig. 9 illustrates the variations in contact diameter, effective diameter, and cutting speed for this case.

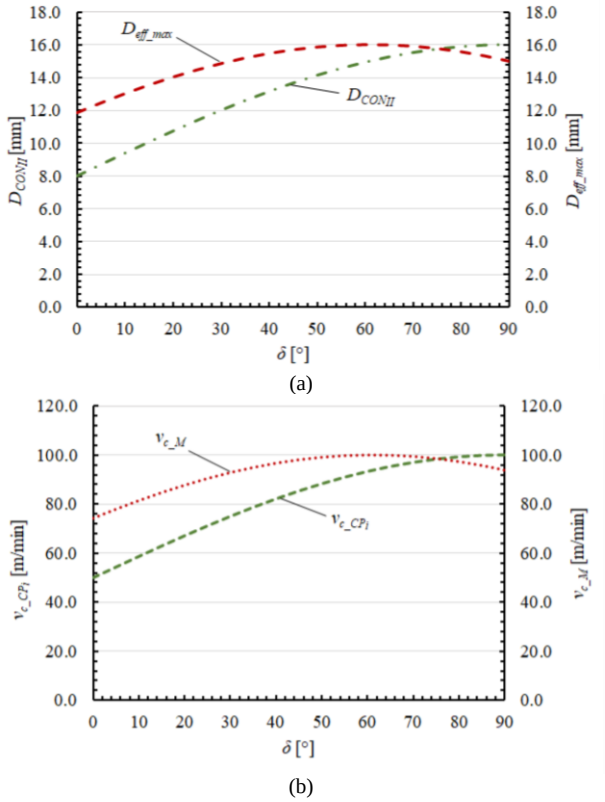

Fig. 9. The changing of: (a) the contact and effective diameters, (b) the cutting speed, in the function of inclination angle δ.

As the value of the angle δ of the torus cutter axis in the feed direction increases, the value of the contact diameter $D_{CON_{II}}$ also increases. The same is true for the cutting speed v_{c_CPi} at the contact point. The minimum values of these parameters are obtained for δ=0°, and the maximum values for δ = 90°. Whereas, as the value of the angle δ in the feed direction increases, the value of the effective diameter D_{eff_max} and the cutting speed v_{c_M}, also increase, before reaching a maximum and these values decrease. This is due to the geometry of the torus. In doing so, two important aspects should be noted. Firstly, the actual cutting speed is always lower than the programmed one because both the contact and effective diameters are smaller than the principal diameter, therefore, for example, for δ=10° instead of 100 m/min a speed of v_{c_Cpi} = 58.68241 m/min and v_{c_M} = 81.43551 m/min is realized. In this case, the difference is 29%, and over the entire δ angle range from 0% to 67%. Secondly, for the torus geometry, there is a special case for which the difference in the values of the tested parameters is 0%. In the machining example being considered, this is the setting for which the angle δ = 75.52249°, and it depends on the radius of the round cutting insert of the torus and the depth of cut. In this case, the contact and effective diameters are equal. On this basis, it can be assumed that the milling will be more beneficial with the smaller the differences between these diameters.

Tests were then carried out for the case in which the machining parameters were set relative to the contact diameter $D_{CON_{II}}$, and therefore directly affect the cutting conditions in the CWE at the CP_i contact point and thus the topography of the shaped surface. Firstly, the courses of: the cutting speed at point M and at point CP_i as a function of inclination angle δ are collated. These courses are illustrated in Fig. 10. From this graph, it was found that by setting the same value of cutting speed at the contact point (100 m/min) for each new angle value, the cutting speed at the limit point M of the cut layer cross section decreases.

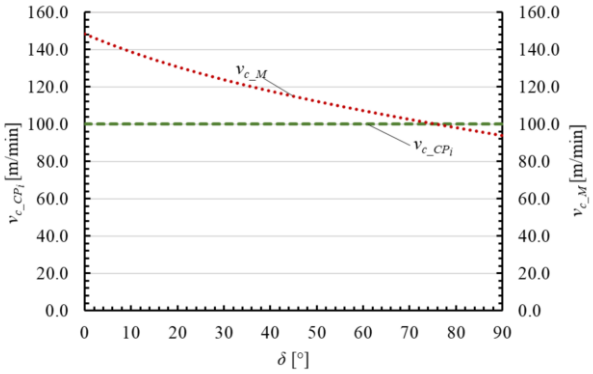

Fig. 10. The changing of the cutting speed at point M and point CP_i in CWE in the function of inclination angle δ.

Furthermore, it should be noted that the cutting speed v_{c_M} occurs in the zone of maximum thickness of the cut layer. Thus, it can be concluded that a decrease in the value of the cutting speed at point M of the cut layer cross-section can significantly increase tool life and reduce the formation of notching wear.

Based on the above, secondly compares the courses of the cutting speed v_{c_CPi} and the feed rate v_f as a function of the inclination angle δ, for machining parameters related to the principal diameter and then the contact diameter. These courses are illustrated in Fig. 11.

From these graphs, it was found that when the machining parameters are fixed with respect to the principal diameter, the cutting speed at the contact point increases as the angle of inclination increases, and the feed rate does not change (top graph). However, when the machining parameters are fixed with respect to the contact diameter, the cutting speed at the contact point does not change and the feed rate (also the spindle speed) decreases (bottom graph). Note that for small inclination angles, the feed rate in the second case is almost twice as high as the feed rate in the first case. This can have a negative impact on the tool life. However, it should be denoted that the cutting speed is the parameter that most

influences the wear of the tool. Higher feed rates, on the other hand, undoubtedly increase the efficiency of the machining process.

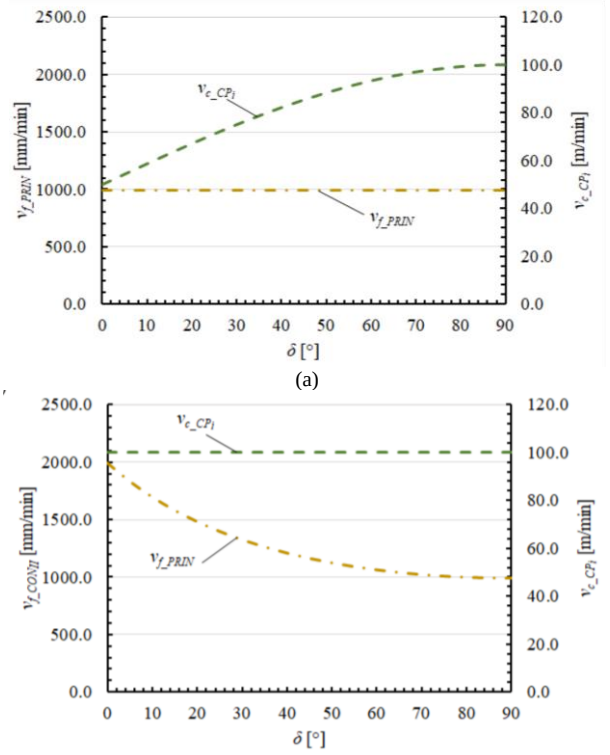

Fig. 11. The changing of: (a) the cutting speed at point CP_i, (b) the feed rate v_{f_PRIN} in CWE, in the function of inclination angle δ.

2) Case, $\delta \geq 0°$ and $0° \leq \theta \leq 90°$

In the next step, the effect of the rotational angle θ of the torus milling cutter axis on the change in contact diameter and effective diameter was investigated. The courses obtained are shown in Fig. 12 for the *DP-TPL*, and Fig. 13 for the *DN-TPL* kinematic variant, respectively.

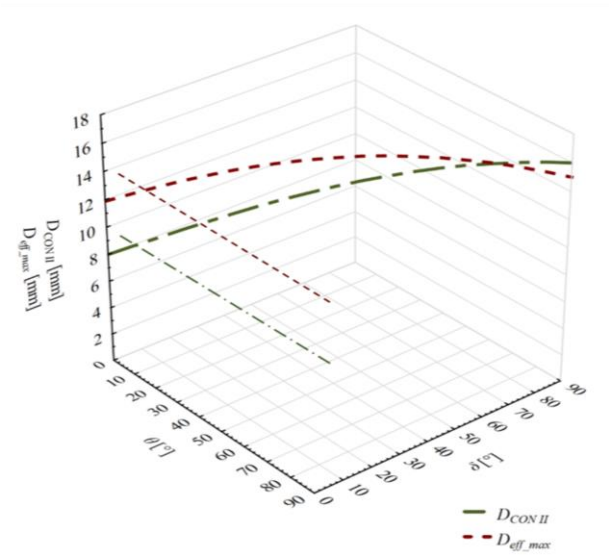

Fig. 12. The changing of the contact and effective diameters in the function of rotational angle in the *DP-TPL* kinematic cutting variant.

Analysing the graphs obtained for both kinematic variants, it was found that the rotational angle of the tool axis has no effect on either changes in contact diameter or changes in effective diameter. At this stage of the research, it can be concluded that the variations in these diameters will generally be influenced by the geometry of the tool used for machining, the curvature of the machined sculptured surface and the uneven distribution of the machining allowance, which translates into variations in depth of cut values along the tool path.

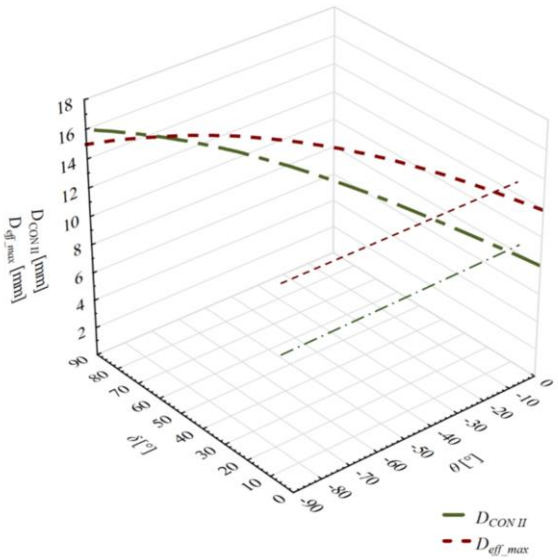

Fig. 13. The changing of the contact and effective diameters in the function of rotational angle in the *DN-TPL* kinematic cutting variant.

B. Changing the Working Angle of the Tool Blade

Fig. 14 illustrates the changes of the work angle ψ_r of the cutter blade as a function of the maximum depth of cut a_{p_max} occurring at the CP_i contact point, whereas Fig. 15 illustrates the changes of the cutter blade work angle ψ_r as a function of the feed per tooth f_z.

By analysing the graphs obtained, it was found that both with an increase in the value of the maximum depth of cut at the contact point and the feed per tooth, the cutter blade work angle increases. This results in an extension of the active cutting edge segment.

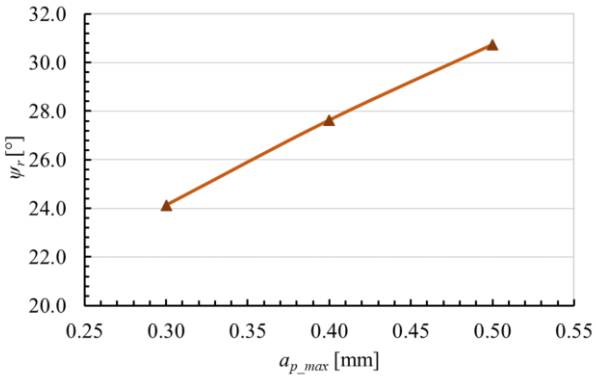

Fig. 14. The changing of the cutting blade work angle in the function of maximal depth of cut.

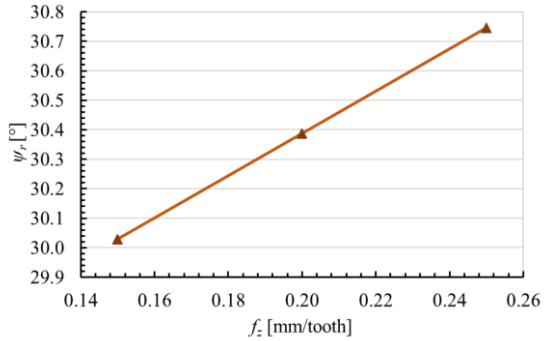

Fig. 15. The changing of the cutting blade work angle in the function of feed per tooth.

Figs. 16 and 17, in turn, illustrate the changes in the cutter blade work angle ψ_r as a function of the rotational angle θ of the tool axis with respect to the contact point CP_i, respectively for the multi-axis kinematic variants *DP-TPL* and *DN-TPL*. The kinematic variant of *TPL* is illustrated in the graphs by the rotational angle θ=90°.

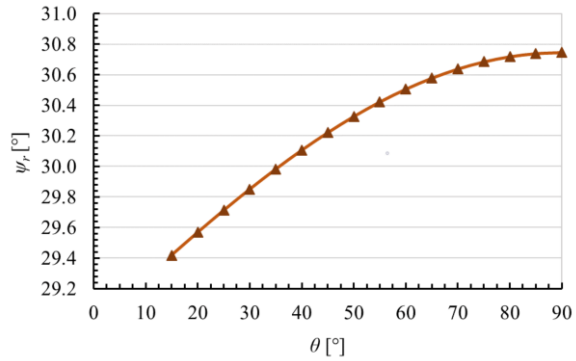

Fig. 16. The changing of the cutting blade work angle in the function of maximal depth of cut.

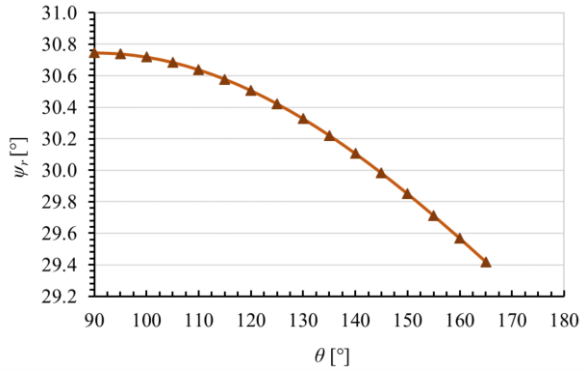

Fig. 17. The changing of the cutting blade work angle in the function of maximal depth of cut.

From the analysis of the graphs above, it can be seen that the rotational angle affects changes in the cutter blade work angle, and thus the length of the active cutting edge segment. The highest value of the cutter blade work angle at the contact point was obtained for the *TPL* variant. The change in the working angle of the cutter blade as a function of the rotational angle of the tool axis is related in this case to a change in the parameter $f_z/2$. This change takes place as a function of the rotational angle in the area defined by the $O_{ci}CP_iE$ points (see Fig. 5). In this area, the cutting edge shapes the part of the roughness profile downstream of the contact point, and this can be important in terms of the minimum thickness of the cut layer. Taking this into account, graphs were developed showing the differences between the maximum value of the parameter $f_z/2$, and the values resulting from the introduction of the rotational angle of the tool axis, i.e., $f_z/2\sin(\theta)$. The graphs are illustrated in Figs. 18 and 19.

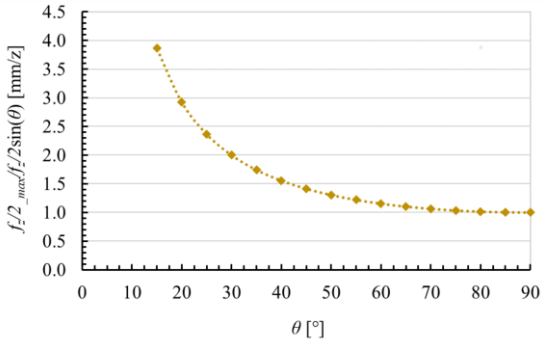

Fig. 18. Course of variation of the ratio ($f_z/2$) / ($f_z/2\sin(\theta)$) as a function of the rotational angle θ for the *DP-TPL* variant.

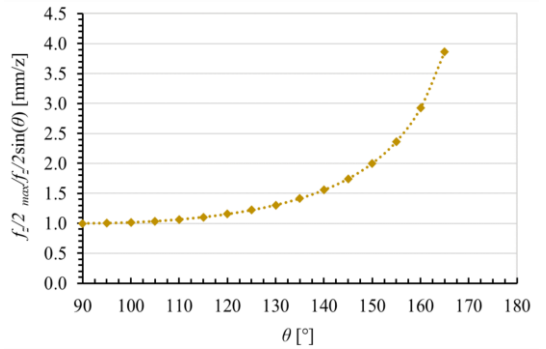

Fig. 19. Course of variation of the ratio ($f_z/2$) / ($f_z/2\sin(\theta)$) as a function of the rotational angle θ for the *DN-TPL* variant.

Figs. 18 and 19 show that the differences between the maximum value of the parameter $f_z/2$, and the values resulting from the introduction of the rotational angle of the tool axis, i.e., $f_z/2\sin(\theta)$, are almost four times, in the range of large values of the rotational angle θ. Whereas, in the kinematic variant of *TPL* multi-axis cutting, the ratio is 1. An increase in the angle θ, whether in the negative or positive direction, results in an increase in the ratio ($f_z/2$)/($f_z/2\sin(\theta)$).

C. Surface Roughness

Histograms of selected 3D surface roughness parameters are illustrated in Fig. 20. Whereas, Fig. 21 illustrates images of machined surfaces and texture images of these surfaces.

From the analysis of the measurement results obtained, it can be seen that in terms of the physical and functional properties of the surfaces obtained, those shaped with the *TPL* kinematic variant are the best.

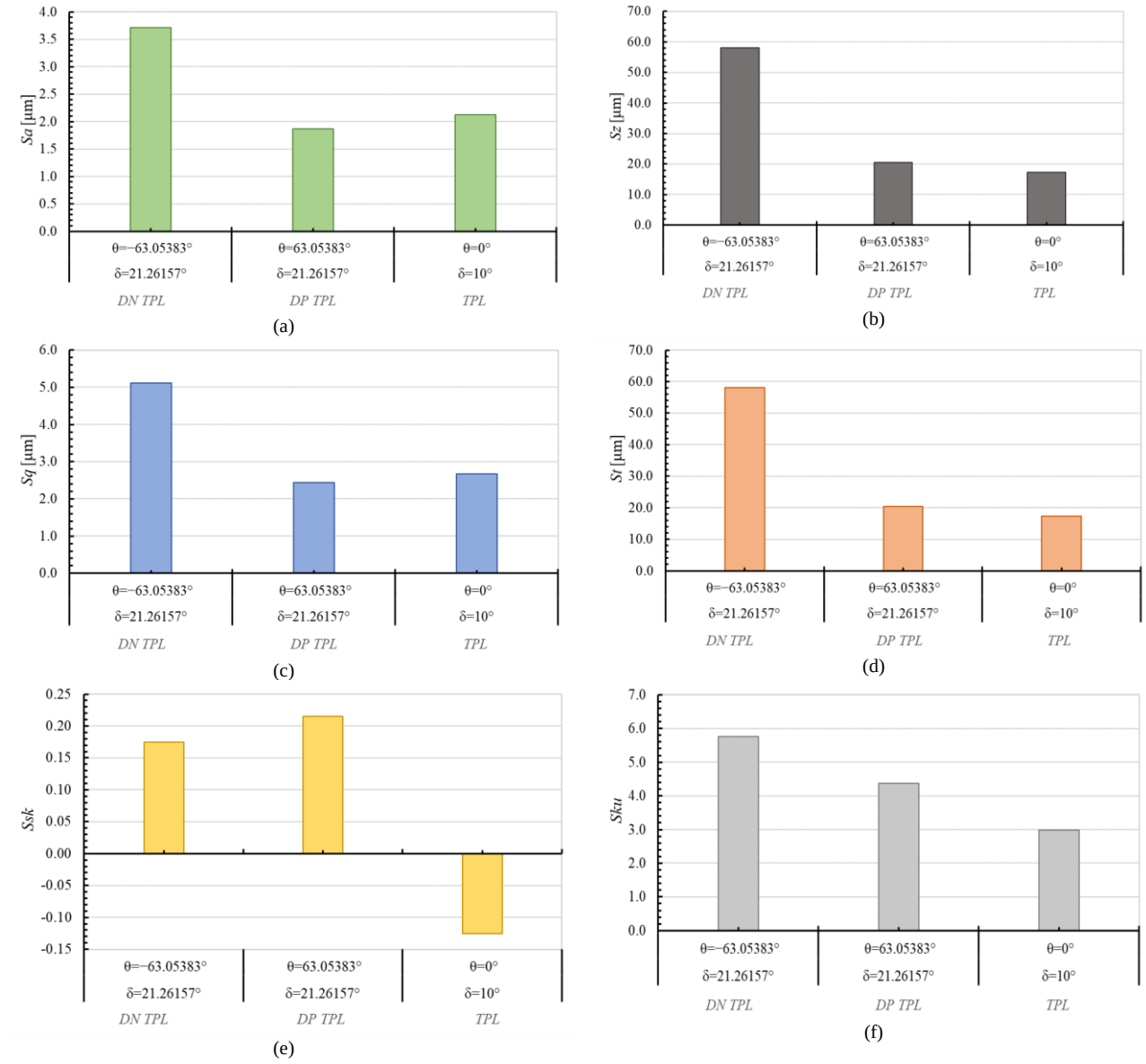

Fig. 20. Histograms of the 3D (area) surface roughness parameters after multi-axis milling using the torus milling cutter with a different kinematic variants cutting: (a) Sa: arithmetical mean height, (b) Sz: maximum hight, (c) Sq: root mean square hight, (d) St: maximum peak hight, (e) Ssk: skewness, (f) Sku: kurtosis.

Surfaces after multi-axis milling with the *TPL* variant are characterised by low roughness, which contributes to fatigue strength. As *Sa* = 2.12 µm, the effect of roughness on fatigue strength is comparable to that of residual stress and microstructure of the material. This is evidenced, among other things, by the parameter *Sku* = 3, which means that the machined surface is characterised by a Gaussian distribution of the shape of the grooves of the surface profile and thus a favourable stress concentration. In addition, the resulting lower surface roughness increases the corrosion resistance of this surface. The structure of these surfaces is characterised by anisotropy, which also makes them more resistant to corrosion. On the other hand, for consumption of *VB* = 0 mm parameter *Ssk* = −0.008, for *VB* = 0.15 mm *Ssk* = −0.12, and beyond *VB* = 0.3 mm *Ssk* = 0.14. This shows that the surface obtained by multi-axis *TPL* milling is flat, has an overall symmetrical height distribution, and contains small indentations. Thus, tool wear also has a strong influence on the physical and functional characteristics of the surfaces manufactured with the *TPL* variant.

D. Tool Wear

As shown in Fig. 22, for the adopted wear criterion of *VB*=0.3 mm, the tool life was 1.33; 1.83 and 3.33 min for the kinematic variant of *DN-TPL*; *TPL* and *DP-TPL* multi-axis cutting, respectively. It can therefore be seen that the change in tribological conditions in CWE resulting from the geometrical-kinematic relationships of multi-axis milling results in an increase in tool life.

By analysing the wear curves, it can be seen that they present a classic three-phase course.

During the inception phase, the wear rate is relatively high, and wear reaches a baseline in a short time. In the middle phase, uniform wear and tear of a quasi-linear and predictable nature can be observed. The final phase is

characterised by accelerated wear until a critical value associated with cutting blade failure is reached.

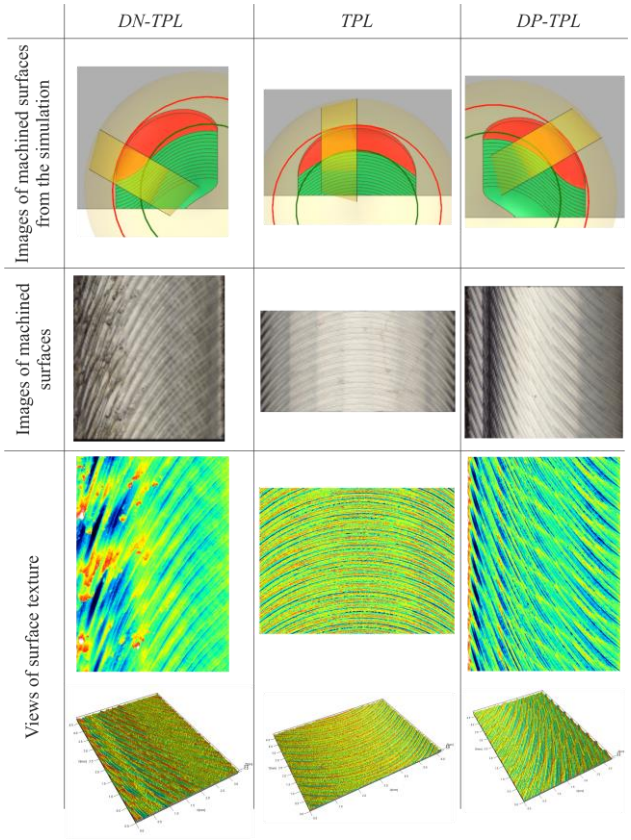

Fig. 21. Images of machined surfaces and views of surface texture after multi-axis milling using the torus milling cutter.

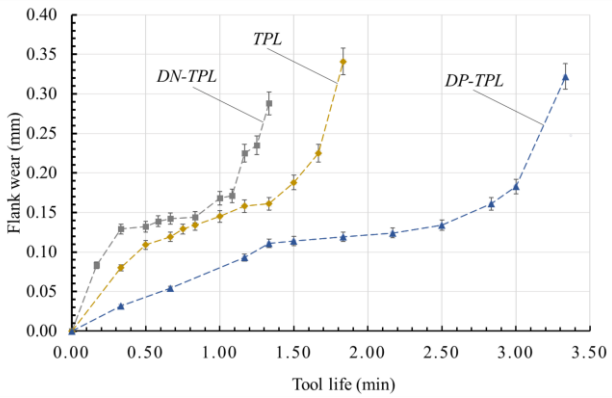

Fig. 22. Change of the wear indicator *VB* on the flank surface of the round cutting insert for multi-axis milling *DN-TPL*, *TPL* and *DP-TPL*.

The contact diameter and effective diameter of the torus milling cutter change continuously when milling sculptured surfaces. Consequently, the actual position of the contact point on the cutting edge of the cutter also changes. Along with this parameter, the cross section of the cut layer, the cutting speed, and the tool life in the CWE also change. It also fundamentally affects surface integrity. To minimise this impact, it is worth considering keeping the contact and effective diameters constant or very slightly varying during toolpath planning and determining the machining parameters in relation to the contact point.

In order to do this, it is necessary to carry out the necessary calculations at any point in the toolpath on the workpiece surface as early as the planning stage of the multi-axis milling process.

VI. Conclusion

This work presents selected the theoretical and experimental issues of the process of multi-axis milling of the surface of Ni-based superalloy Inconel 718 parts used the torus milling cutter in a kinematic variants of the: tool pulling, diagonal positive tool pulling, and diagonal negative tool pulling types, in terms of surface quality and tool wear. Since cutting speed during high-speed finishing milling is the parameter that has the greatest impact on tool life and surface roughness, mathematical models of the contact diameter and effective diameter were first developed. Simulations and experiments of multi-axis milling were carried out, and the necessary analyses were performed. It is worth highlighting that the theoretical and experimental research was based on the parameter of the working angle of the tool blade in the basic plane, which is very rarely taken into account. This is a novelty in the geometric-kinematic approach to determining technological, geometric, and physical parameters within of the cutting layer. The following conclusions were drawn from the results obtained.

The value of the contact diameter basically depends on the radius of the torus milling cutter, the radius of the round cutting insert, and the inclination angle of the torus milling cutter axis. The contact curve is also part of the trajectory of the contact point within the cutting layer. Whereas, the value of the effective diameter depends essentially on the radius of the torus cutter, the radius of the round cutting insert, the angle of inclination of the torus cutter axis and the boundary angle of the intersection point of the cutting edge outline with the pre-finished surface outline. In the CWE area, there are significant changes in the cutting speed values.

It was found that when the machining parameters are fixed with respect to the principal diameter, the cutting speed at the contact point increases as the angle of inclination increases and the feed rate does not change. However, when the machining parameters are fixed with respect to the contact diameter, the cutting speed at the contact point does not change and the feed rate (also the spindle speed) decreases with an increase in the inclination angle.

In addition, it was found that the rotational angle of the tool axis affects changes in the tool blade working angle, and thus the length of the active cutting edge segment. The change in the working angle of the tool blade as a function of the rotational angle of the tool axis is related to a change in the parameter $f_z/2$. Hence, climb milling was obtained for the variants tool pulling and diagonal positive tool pulling, whereas for the variant diagonal negative tool pulling conventional milling was obtained.

The best results of machining tests, taking into account the obtained values of surface roughness and tool life

parameters, were obtained for the variant tool pulling, and thus this kinematic variant of the multi-axis milling requires conducting further research in the field of physical and technological aspects of cutting.

CONFLICT OF INTEREST

The author declares no conflict of interest.

ACKNOWLEDGMENT

I would like to thank Anna Bazan for her help in surface roughness measured of the research objects.

REFERENCES

[1] C. Zhang, S. Guo, H. Zhang, and L. Zhou, "Modeling and predicting for surface topography considering tool wear in milling process," *Int. J. Adv. Manuf. Technol.*, vol. 68, no. 9–12, pp. 2849–2860, Oct. 2013.

[2] L.-X. Cao, H. Gong, and J. Liu, "The offset approach of machining free form surface," *Journal of Materials Processing Technology*, vol. 184, no. 1–3, pp. 6–11, Apr. 2007.

[3] M. Gdula, "Empirical models for surface roughness and topography in 5-axis milling based on analysis of lead angle and curvature radius of sculptured surfaces," *Metals*, vol. 10, no. 7, 932, Jul. 2020.

[4] M. Gdula and J. Burek, "Cutting layer and cutting forces in a 5-axis milling of sculptured surfaces using the toroidal cutter," *Journal of Machine Engineering*, vol. 4, no. 17, pp. 98–122, Dec. 2017.

[5] Z. Chang, J. Qian, Z. C. Chen, N. Wan, and D. Zhang, "Geometrical theory of cutting stock with torus end mills in five-axis CNC machining and its applications in machining simulation," *Int. J. Adv. Manuf. Technol.*, vol. 105, no. 1–4, pp. 27–46, Nov. 2019.

[6] Z. Zhu, F. Peng, R. Yan, Z. Li, J. Wu, X. Tang, and C. Chen, "Influence mechanism of machining angles on force induced error and their selection in five axis bullnose end milling," *Chinese Journal of Aeronautics*, vol. 33, no. 12, pp. 3447–3459, Dec. 2020.

[7] J. Fan, "Cutting speed modelling in ball nose milling applications," *Int. J. Adv. Manuf. Technol.*, vol. 73, no. 1–4, pp. 161–171, Jul. 2014.

[8] A. F. De Souza, A. E. Diniz, A. R. Rodrigues, and R. T. Coelho, "Investigating the cutting phenomena in free-form milling using a ball-end cutting tool for die and mold manufacturing," *Int. J. Adv. Manuf. Technol.*, vol. 71, no. 9–12, pp. 1565–1577, Apr. 2014.

[9] S. Wojciechowski, P. Twardowski, and M. Wieczorowski, "Surface texture analysis after ball End milling with various surface inclination of hardened steel," *Metrology and Measurement Systems*, vol. 21, no. 1, pp. 145–156, Mar. 2014.

[10] S. Wojciechowski and P. Twardowski, "The influence of tool wear on the vibrations during ball end milling of hardened steel," *Procedia CIRP*, vol. 14, pp. 587–592, 2014.

[11] S. Wojciechowski and P. Twardowski, "Tool life and process dynamics in high speed ball end milling of hardened steel," *Procedia CIRP*, vol. 1, pp. 289–294, 2012.

[12] B. Mikó and P. Zentay, "A geometric approach of working tool diameter in 3-axis ball-end milling," *Int. J. Adv. Manuf. Technol.*, vol. 104, no. 1–4, pp. 1497–1507, Sep. 2019.

[13] A. Mgherony and B. Mikó, "Simulation of the working diameter in 3-axis ball-end milling of free form surface," *Teh. Vjesn.*, vol. 29, no. 4, Aug. 2022.

[14] T. Vopát, J. Peterka, V. Šimna, and M. Kuruc, "The influence of different types of copy milling on the surface roughness and tool life of end mills," *Procedia Engineering*, vol. 100, pp. 868–876, 2015.

[15] A. V. Vyboishchik, "Modelling topology of freeform surfaces with ball-end milling," *Procedia Engineering*, vol. 150, pp. 761–767, 2016.

[16] J. Beňo, I. Maňková, P. Ižol, and M. Vrabel', "An approach to the evaluation of multivariate data during ball end milling free-form surface fragments," *Measurement*, vol. 84, pp. 7–20, Apr. 2016.

[17] A. E. Pena, F. D. Anania, and M. Zapciu, "Research concerning optimum cutting parameters according with tool path strategy for finishing procedures," *IOP Conf. Ser.: Mater. Sci. Eng.*, vol. 95, 012020, Nov. 2015.

[18] Pena, "Method for optimum calculus of machining parameters according to tool trajectories type based on milling process simulation," *Teh. Vjesn.*, vol. 24, no. 2, Apr. 2017.

[19] J.-M. Redonnet, A. G. Vázquez, A. T. Michel, and S. Segonds, "Optimization of free-form surface machining using parallel planes strategy and torus milling cutter," in *Proc. the Institution of Mechanical Engineers, Part B: Journal of Engineering Manufacture*, Jan. 2018, vol. 232, no. 2, pp. 240–250.

[20] Q. Zhang, S. Zhang, and W. Shi, "Modeling of surface topography based on relationship between feed per tooth and radial depth of cut in ball-end milling of AISI H13 steel," *Int. J. Adv. Manuf. Technol.*, vol. 95, no. 9–12, pp. 4199–4209, Apr. 2018.

[21] X. Liu, Y. Li, and Q. Li, "A region-based 3 + 2-axis machining toolpath generation method for freeform surface," *Int. J. Adv. Manuf. Technol.*, vol. 97, no. 1–4, pp. 1149–1163, Jul. 2018.

[22] M. Gdula and G. Mrówka-Nowotnik, "Analysis of tool wear, chip and machined surface morphology in multi-axis milling process of Ni-based superalloy using the torus milling cutter," *Wear*, vol. 520–521, 204652, May 2023.

[23] A. Mgherony and B. Mikó, "Controlling the spindle speed when milling free-form surfaces using ball-end milling cutter," *Acta Polytech Hung*, vol. 20, no. 6, pp. 135–149, 2023.

[24] A. Mgherony and B. Mikó, "The effect of the cutting speed on the surface roughness when ball-end milling," *Hung. J. Ind. Chem.*, vol. 49, no. 2, pp. 9–13, 2021.

[25] A. Mgherony and B. Mikó, "The effect of the spindle speed control when milling free-form surfaces," *Int. J. Adv. Manuf. Technol.*, vol. 130, no. 3–4, pp. 1439–1449, Jan. 2024.

[26] A. Mgherony and B. Mikó, "Tool path planning of ball-end milling of free-form surfaces as a search algorithm," *Acta Tech. Jaurinensis*, Mar. 2024.